Materials Research Proceedings 41 (2024) 2075-2084 https://doi.org/10.21741/9781644903131-229

Applying images processing methods for automation measurement of tool-chip contact length in orthogonal cutting

FAVIER Camille[1,a], LE ROUX Julien[1,b], CALAMAZ Madalina[1,c*], GIRARDOT Jérémie[1,d] and LIMJE Preshit[1,e]

[1]Arts et Metiers Institute of Technology, CNRS, Bordeaux INP, Hesam University, I2M, UMR 5295, F-33400, Talence, France

[a]camille.favier@ensam.eu, [b]julien.le_roux_1@ensam.eu, [c]madalina.calamaz@ensam.eu, [d]jeremie.girardot@ensam.eu, [e]preshitlimje24@gmail.com

Keywords: Chip Formation, Images Processing, Tool-Chip Contact Length

Abstract. The simulation of machining process is an essential tool in the digitalization of the entire production chain. Currently, these simulations are not sufficiently precise to avoid the use of experimental tests in order to optimize machining operations and guarantee the quality of the machined parts. Some parameters, such as tool-chip contact length, are still underestimated, although they are critical for controlling heat transfer into the tool and implicitly its wear. In order to validate a numerical cutting simulation model, the tool-chip contact length experimentally measured should be used as a comparative quantity, in the same way as the cutting forces and the morphology of the chips is currently used. The objective of this paper is to propose an automation of tool-chip contact length measurements using image processing algorithms. The proposed algorithm was able to identify and measure the tool-chip contact length on more that 75% of images. The algorithm accuracy is evaluated by comparing computed and manually measured tool-chip contact length, for different cutting conditions. It was found that it overestimates the contact length, especially in the case where the image quality is lower.

Introduction

Machining simulations are pivotal in the digital transformation of the entire production chain. However, current simulations lack the precision to replace experimental tests for optimizing operations and ensuring the quality of machined parts. The use of cutting forces and chips morphology experimentally obtained has become a commonly implemented practice to validate numerical simulation models of orthogonal cutting. Certain parameters, notably measured tool-chip contact lengths, are less often used for comparison in numerical simulations, and when they are used, it turns out to remain underestimated. Particular attention should be paid to this metric, as it plays a critical role in controlling heat transfer into the tool and its consequent wear. To validate numerical cutting simulation models, experimentally measured tool-chip contact length should be utilized as a comparative metric, similar to how cutting forces and chip morphology are presently employed.

Tool-chip contact length (Lc) is measured in two different ways: i) by measuring the imprint left by the chip on the tool rake face or ii) on images from video recording of cutting process. Storchak et al. [1] carried out orthogonal cutting tests on an AISI 1045 steel workpiece using various cutting speeds, uncut chip thicknesses and tool rake angles. Cutting forces and tool-chip contact length were measured and compared to those provided by numerical simulation of cutting. The purpose of their study was to find out the main parameters of the material behaviour law used in numerical simulation of cutting that influence the prediction of Lc. The chip formation during cutting was recorded using a video camera. Contact length was manually measured on images and associated numerical model served as a benchmark for comprehending variations in Lc. Sutter [2] delved into chip geometries during high-speed machining, employing a ballistic device for

orthogonal cutting conditions. The tool-chip contact length measurements were carried out using the software that controls the camera and enables the enhancement of specific contrasts only. Their experimental scrutiny of tool-chip contact length and shear angle provided insights into machining dynamics across varying speed and depths of cut.

Iqbal et al. [3] executed a comparative study on tool-chip contact length in turning for two engineering alloys (an AISI 1045 steel and a Ti6Al4V titanium alloy), introducing new models tailored for high-speed machining. To measure the contact length, cutting inserts were analysed using a Polyvar optical microscope equipped with image processing software. The contact marks left by the chip on the tool rake face were employed to identify the contact area. The study underscored how machinability influences the prediction of Lc, crucial for understanding heat transfer and wear models.

Ellersiek et al. [4] evaluated methods for measuring tool-chip contact length in wet machining, introducing innovative approaches such as the use of microtextured tools. The micro-textures were implemented on the tool's rake face in the direction of chip flow on the insert. This facilitates the determination of the contact length using laser textures applied at a steadily increasing angle. The initial micro-texturing is positioned 210 μm away from the tool cutting edge, meaning that only contact lengths beyond this distance can be detected. Following that, the undersides of the resulting chips at three distinct locations: beginning, middle, and end of the cutting were examined using topography images to obtain statistical validation. Also, in-situ visualization with high-speed recordings study, knowing the pixel size, was carried out, and compared to the results from the microtextured tool approach. The study accentuates the challenges in determining contact length in wet conditions, essential for comprehending the chip formation process.

Klippel et al. [5] introduced an automated chip characteristics determination method, measuring thickness and curling radius, automatically derived from images of the chips through image processing, encompassing image preparation and contour detection. These automated measurements are then compared to manually obtained data. A Convolutional Neural Network was introduced to automate the decision-making process regarding the application of algorithms for continuous chips (utilizing average chip thickness) or segmented chips (considering minimum and maximum chip thicknesses along with chip segment lengths). The study aimed to determine average chip thickness, curling radii and segmentation lengths, laying the groundwork for automated chip analysis.

Qazani et al. [6] proposed a prediction model of tool-chip contact length using an adaptive network-based fuzzy inference system (ANFIS) in orthogonal cutting of an AISI 4140 steel. To train and test the proposed models, a dataset of tool-chip contact length was created manually, for different machining conditions, using images captured with a microscope and imported in the image processing software *Clemex*. The experiments were conducted three times, and the average value for the tool–chip contact length was chosen during the analysis. The study focused on leveraging machine learning methods to predict Lc, showcasing the potential of ANFIS in enhancing accuracy. Arefin et al. [7] delved into chip formation mechanisms in one-dimensional vibration-assisted machining (VAM), uncovering the intermittent nature of cutting in VAM. Both orthogonal cutting simulations and experiments were carried out. Each test was conducted five times minimum to ensure repeatability and confirmation of the measurements, in terms of forces and chip dimensions (determined with a Scanning Electron Microscope). Their findings reveal a smaller tool-chip contact length in VAM compared to conventional machining, impacting chip thickness.

Gzresik [8] proposed a computer-based technique to determine more accurately the tool-chip contact length, using image processing methods applied to images of tool rake face. The image processing was based on scaling, image contrast improving and colour filtering. As a result, both the tool–chip contact length and the actual area of contact were determined more accurately than

by using an optical microscope in the post-cutting stage. This aims to estimate the real contact area between the rake face and the sliding chip, ensuring a more precise determination of contact loads and heat fluxes. The study revealed a potential difference of approximately 25% between the actual and nominal contact areas.

Barelli et al. [9] proposed an identification of tool-chip contact length in a Ti6Al4V titanium alloy turning, using image processing. An image pre-treatement was first applied, enhancing contrast on raw images, in order to highlight the tool and the chip. A 255 (white colour) grayscale value is attributed to the tool and 0 (black colour) to its edge. Then, by employing image processing techniques, the tool-chip contact length was automatically discerned in a provided pretreated image. This was achieved through the initial identification of the tool tip and cutting edge, utilizing contour coordinates and modifying the grayscale of the image.

This study aims to automate the recognition of the separation point between the tool rake face and the chip, using diverse images recorded during orthogonal cutting of a titanium alloy. Tool-chip contact length is measured on a minimum of 100 images for each machining condition. The accuracy of the algorithm is evaluated by comparing computed and manually measured tool-chip contact lengths. The evolution of tool-chip contact length with respect to uncut chip thickness and cutting speed is then evaluated.

Experimental setup and cutting conditions

Chip formation during orthogonal cutting was recorded by a high-speed video camera (Photron SA5). A long-distance microscope (Questar QM100) was used to observe the chip-forming zone in front of the cutting tool. The scene is illuminated by a fiber-optic lighting system. The optical setup and machine configuration are illustrated in Fig. 1a.

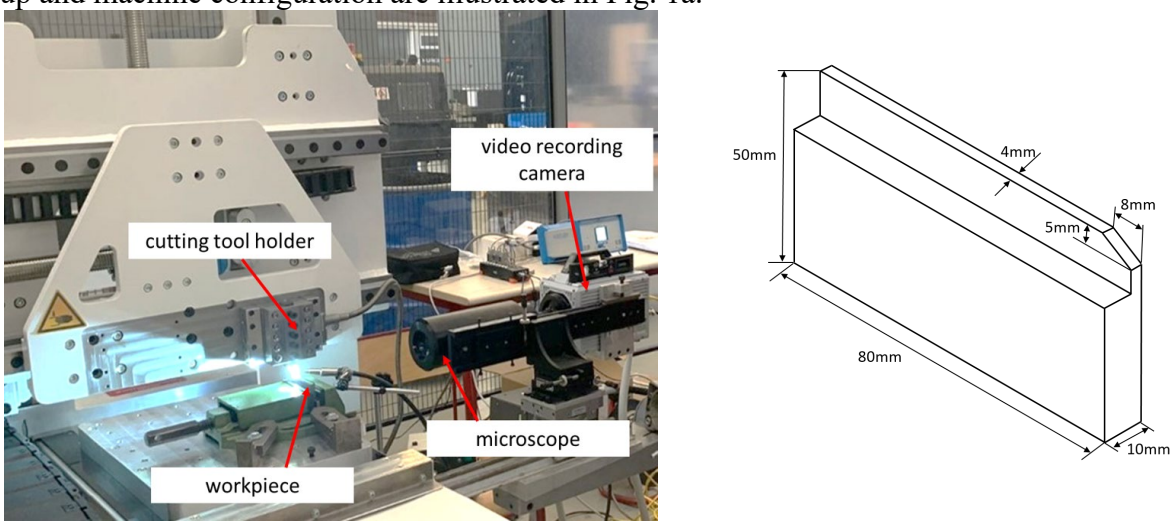

a) b)

Fig. 1. a) experimental setup; b) workpiece dimensions

The machined part is a Ti6Al4V titanium alloy plate; its dimensions are shown in Fig. 1b. The cutting tool is made of tungsten carbide (CW-6%Co); it has a cutting angle of 0°, a clearance angle of 7° and an edge radius of about 20µm. The workpiece is mounted in a vice, which is attached on the machine table. The cutting speed is given to the machine table and the tool is held stationary. The cutting speeds (Vc) used for this study are: 30, 45 and 60m/min and the uncut chip thicknesses (h) are of 0.1mm and 0.2mm respectively. The resolution of the camera is of 768x648 pixels for all tests performed with the uncut chip thickness of 0.1mm, and it is of 1024x496 pixels for those with a 0.2mm uncut chip thickness. The acquisition frequency is of 15 000 frames/sec for all machining conditions used in this study.

Image processing methodology

In the images depicting the formation of chips during machining, it is challenging to accurately discern the extent of contact between the cutting tool and the chip within the images captured by the camera (Fig. 2a). This difficulty predominantly arises due to the presence of shadows caused by the light position, which was not coaxially placed with respect to the optic axe, and some shadow area is formed in front of the tool. Therefore, to improve images clarity, the image processing methodology illustrated in Fig. 2 was applied.

Initially, a *Gaussian filter* was utilized to reduce noise and smoothen the image. An example of the resulting image in shown in Fig. 2b. A Gaussian blur is applied: it is a low-pass filter that convolves the image with a Gaussian function, smoothing out high-frequency noise while preserving the overall structure and edges. By convolving the image with a Gaussian kernel, the filter reduces the impact of high-frequency components, effectively blurring or smoothing the image. This process helps to remove random variations or noise present in the image, that can interfere with the edge detection process, leading to false edges or erroneous results. This Gaussian blurring helps in suppressing small-scale details or insignificant edges that might not be of interest [10].

Gaussian blur is commonly favoured in various applications requiring noise reduction while preserving crucial details and edges in images. This preference stems from its characteristic gradual decrease in influence away from the kernel's centre. This weighting scheme allows for a better preservation of edges in comparison to average smoothing techniques. However, it can also lead to a loss of sharpness, especially in areas with important details or edges [11].

Following this, a *Sobel filter* was employed to emphasize edges and gradients, aiming to enhance the definition between the tool and the chip (Fig. 2c). The Sobel filter emphasizes edges by accentuating the differences in pixel intensity between neighbouring pixels. It calculates the rate of change of intensity and thereby identifies areas in the image where there is a significant change or sharp transition in intensity values. The Sobel operator consists of two convolution kernels: one for detecting horizontal changes and another for vertical changes. These kernels calculate the gradient approximation in the horizontal and vertical directions, respectively, by performing convolution operations on the image. Two separate gradient images are obtained, which can be combined or used independently to highlight and analyse edges [12].

The Sobel filter can be sensitive to noise in an image. High-frequency noise can lead to false edges detection [13]. To prevent these false edges being detected, a *binary thresholding* process was implemented to segment the image and highlight specific areas of interest, facilitating a clearer detection of the tool-chip contact (Fig. 2d). Binary thresholding involves converting the grayscale image into a binary image by setting a threshold value. Pixels with intensity values above the threshold are assigned one value (white), while pixels below the threshold are assigned another value (black), creating a high contrast representation [14].

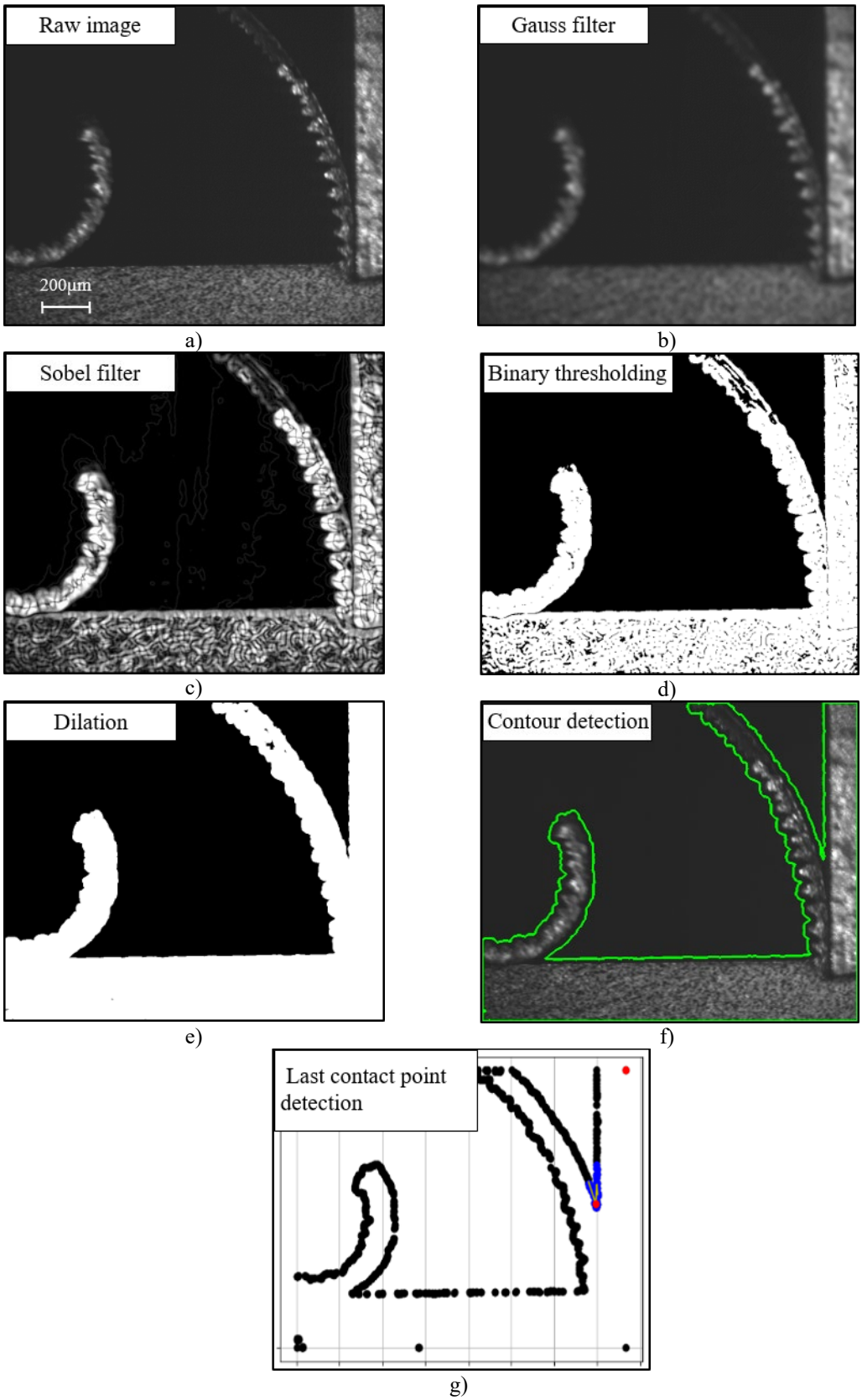

Fig. 2. Different steps of the considered image processing: a) raw image; b) Gauss filter c) Sobel filter d) Binary thresholding e) Dilation f) Contour detection g) Last contact point detection

A sensitivity study was carried out to establish the threshold value to be applied to all images, whatever the machining condition used in this study. A threshold value of 35 enabled to clearly detect the chip, the tool, and the workpiece.

Lastly, a *dilation filter* was used (Fig. 2e). The dilation filter can join or connect disparate elements within an image. It helps in merging separate regions or broken parts of objects present in an image. For each pixel in the image, this operation considers the neighbourhood defined by the structuring element. If the centre pixel of the structuring element overlaps with any part of an object in the image, that pixel is set to the maximum intensity value found within the neighbourhood. As a result, it connects broken parts of an object, fills in gaps, and generally expands the areas identified by the structuring element [15].

Now that a black and white image is obtained, the next step is to apply a function for *edges detection*. The function utilised in this study is "`findContours()`" from OpenCV python library; it takes in a binary image, where the objects are white and the background is black, and returns a list of contours found in the image. Each contour is represented as a list of points that form the boundary of an object [16].

Contours are represented as lists of coordinate points, delineating the combined boundaries of the tool, the chip and the workpiece. After finding the contour (Fig. 2f), the objective is the automated detection of the last contact point between the tool and the chip. Assuming a closed contour oriented in trigonometric direction, the process involves identifying, for each image (and consequently, each contour), the red point in the top right hand of the contour (visible in Fig. 2g).

Following the determination of this point, a specific contour segment (highlighted in blue in Fig. 2g) is chosen, ensuring it encapsulates the last contact point between the tool and the chip. To accomplish this, an analysis of the ordinate evolution along the contour is conducted, and a set of points containing the targeted breakpoint (representing the last point of contact between the tool and the chip) is selected. Subsequently, a piecewise linear regression method is applied to the identified contour using the Python library *pwlf*, as detailed in [17]. The input comprises the 1-D data representing the coordinates of the relevant contour, along with a specified number of line segments (three in this case). The output yields distinct fitting linear parameters for each segment and the identified breakpoints, indicating the boundaries between the different line segments.

Then, the point of interest is designated as the identified breakpoint with the lowest ordinate, and this point is recorded in a dataset as the conclusive last contact point between the tool and the chip for a given input image. Finally, the actual tool-chip contact length is determined for each image by subtracting the ordinate of the tool basis. This specific point is manually assessed using the image processing software PFV4 for each cutting condition and the corresponding series of images.

Results and discussion

Accuracy of the algorithm

In this investigation, the focus is on quantifying the uncertainty associated with measurements automatically conducted by the algorithm. To achieve this, a comparative analysis was conducted by juxtaposing these automated measurements with manually acquired data, as depicted in Fig. 3a and 3b. Manual measurements were made on selected images from a series, using the PFV4 image processing software.

A comparison of measurements was executed for two different uncut thicknesses, revealing an offset in both scenarios: approximately 50 pixels for an uncut chip thickness of 0.2mm (resulting in a 17.8% relative error) and around 100 pixels for an uncut chip thickness of 0.1mm (yielding a 30% relative error), depending on images quality. A prior study by Grzesik [8] concluded that actual and nominal dimensions studied using image processing could exhibit variations of about 25%.

In some cases, both human eye and the algorithm detect the last contact point in roughly the same place, as shown in Fig. 4a. To elucidate the observed offset across all cutting conditions, an in-depth study was conducted, analyzing the images at each step of the image processing pipeline. Notably, human-eye assessments differed between raw images (without any processing) and images after applying the Sobel filter. The Sobel filter revealed previously concealed aspects of the tool and the chip, apparently hidden in the shadows in front of the tool in the raw image, effectively filling the black areas surrounding the tool; therefore, the algorithm positions the tool-chip last contact point at higher y-coordinate (visible on Fig. 4b and c). This discrepancy can be partially attributed to the experimental setup. Given the placement of the lamp on the right side of the tool and the potential coverage of the area of interest by its shadow. Manual measures involve some errors due to the difficulty of perceiving the last contact point, whereas the algorithm, employing various filters, could eventually detect and highlight the chip in shadowed area, imperceptible to the human eye. Therefore, the accuracy of the proposed method will be increased on images coaxially illuminated. Another factor could be the insufficient tuning of the filters for the presented problem, causing excessive modification of the images and resulting in a dilation of the tool and chip.

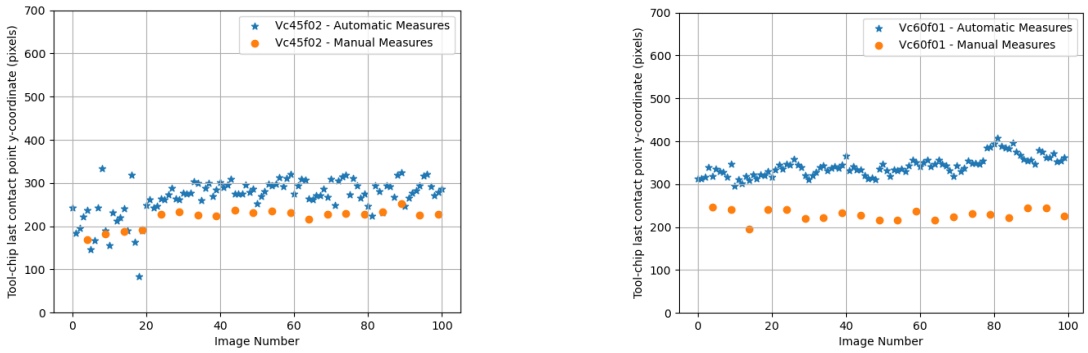

a) b)

Fig. 3. Y-coordinates of tool-chip last contact point vs image number, automatically and manually measured for a) Vc = 45m/min and h = 0.2mm; b) Vc = 60m/min and h = 0.1mm.

Once manual measurements are validated for accuracy, an optimization process can be initiated to fine-tune filter parameters, ensuring the reliability of fully automatic measurements. In conclusion, this underscores the substantial impact of various filters, their tuned parameters, and the experimental setup (including light intensity and orientation), as well as image recording parameters (frame rate and resolution), on the observed differences relative to human measures.

Tool-chip contact length evolution with machining conditions

Fig. 5 illustrates the values of tool-chip contact length automatically measured on sets of 100 images. On some images, the algorithm is unable to consistently identify the last point of contact, resulting in outliers. This is the case for the cutting conditions Vc = 30m/min, h = 0.2mm, on the first 25 images (Fig. 5a) and for Vc = 60m/min, h = 0.2mm, on the first 10 images (Fig. 5b).

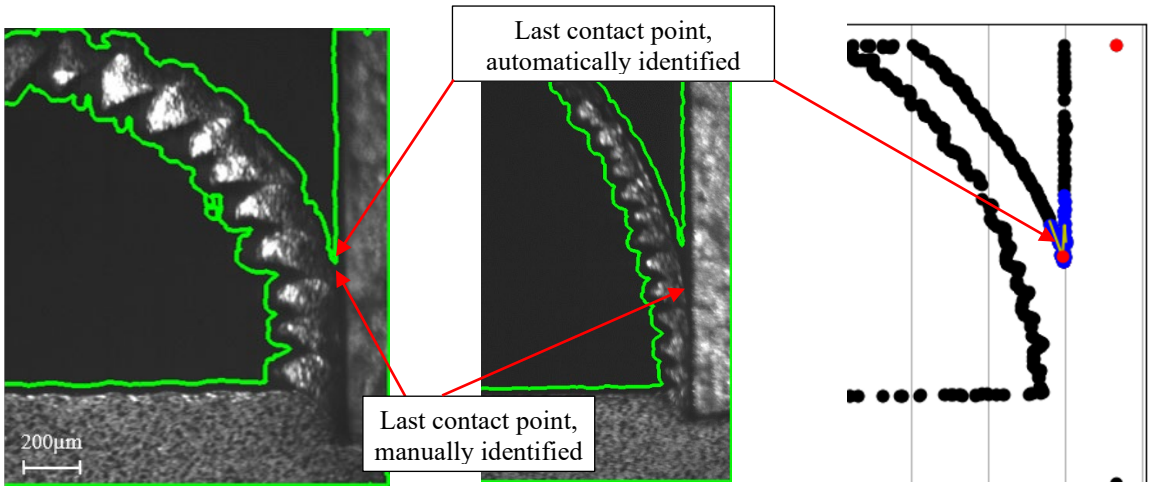

Fig. 4. Examples of the position of the last contact point manually and automatically identified. Contour detection for a) Vc = 45m/min; h = 0.2mm; b) Vc = 60m/min; h = 0.1mm and c) last contact point detection for Vc = 60m/min; h = 0.1mm

For all cutting speed utilised in this study, the tool-chip contact length increases when increasing the uncut chip thickness. Iqbal et al. [3] measured a Lc of 200µm for an h = 0.1mm and a Lc of 400µm for an h = 0.2mm, after machining a titanium alloy with a tool having a rake angle of 0° and with a cutting speed of 60m/min. These values are much lower than those measured in the current study. In the research of Iqbal et al. [3], the Lc was measured on the tool rake faces, which leads to an underestimation of Lc. Concerning tool-chip contact evolution when increasing the uncut chip thickness, a similar trend is found.

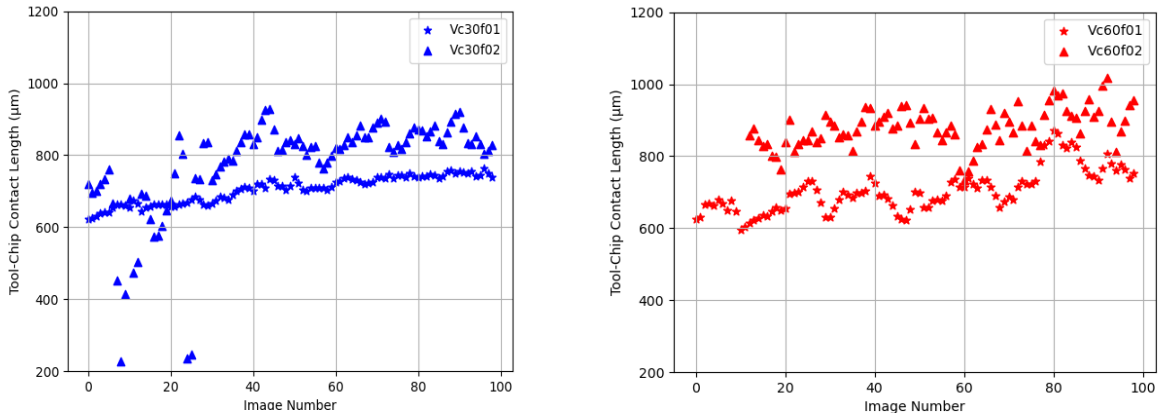

Fig. 5. Tool-chip contact length vs image number for h of 0.1 and 0.2 mm and a) Vc = 30m/min and b) Vc = 60m/min.

In Fig. 5, it can also be observed an increase of the tool-chip contact length between the first and last images of each dataset. In the case of machining using an uncut chip thickness of 0.1mm, an increase of about 19% is noted, for both cutting speeds illustrated in Fig. 5. Nevertheless, this falls within the measurement error range and therefore needs to be further investigated, on other sets of images taken at different stages of the machining process.

Fig. 6 shows the tool-chip contact lengths automatically measured on sets of 100 images, for different cutting speeds. For the speed range considered in this study, there is no real change in contact length with respect to cutting speed, for both uncut chip thicknesses. This trend was also found in [3], for machining with and uncut chip thickness of 0.1mm.

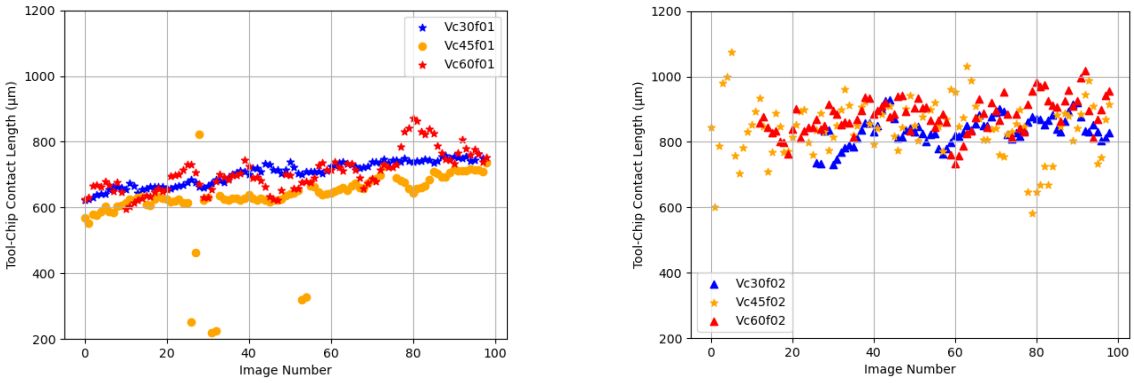

a) b)

Fig. 6. Tool-chip contact length vs image number for a) h=0.1mm and b) h=0.2mm, for different cutting speeds.

Conclusion

In this study, a method for automatic detection of the separation point between the tool rake face and a titanium alloy chip was implemented. This was applied on diverse images recorded during orthogonal cutting. The identification of the tool-chip separation point then allowed the measurement of the contact length. The accuracy of the algorithm was evaluated by comparing computed and manually measured tool-chip contact lengths. The evolution of tool-chip contact length with respect to uncut chip thickness and cutting speed was also evaluated.

The proposed method was able to detect chip, workpiece and tool contours and therefore the last contact point between the chip and the tool. The uncertainty of the automatic measurements was evaluated in relation to manual measurements on raw images. A maximum 30% relative error was found ; this could be attributed to different factors, among which light intensity and its orientation in relation to the cutting tool. The use of a more adapted positioning of the lighting system will enable the recording of images with no shadows in the area of interest. These will be done in a further research work.

For all cutting speed utilised in this study, the tool-chip contact length increases when increasing the uncut chip thickness and no clear evolution was found when increasing the cutting speed.

As the proposed method detects chip contour, automated measurement of its corresponding parameters (thickness - for a ribbon like chip and number of segments-in the case of a serrated chip) could be considered in a future work, on higher quality chip formation images.

References

[1] M. Storchak, K. Drewle, C. Menze, T. Stehle, H.-C. Möhring, Determination of the Tool–Chip Contact Length for the Cutting Processes, Materials 15 (2022) 3264. https://doi.org/10.3390/ma15093264

[2] G. Sutter, Chip geometries during high-speed machining for orthogonal cutting conditions, International Journal of Machine Tools and Manufacture 45 (2005) 719–726. https://doi.org/10.1016/j.ijmachtools.2004.09.018

[3] S. Ahasan Iqbal, P. T. Mativenga, M. A. Sheikh, A comparative study of the tool–chip contact length in turning of two engineering alloys for a wide range of cutting speeds, Int. J. Advanced Manufacturing Technology, 42 (2009) 30-40. https://doi.org/10.1007/s00170-008-1582-6

[4] L. Ellersiek, C. Menze, F. Sauer, B. Denkena, H.-C. Mohring, V. Schulze, Evaluation of methods for measuring tool-chip contact length in wet machining using different approaches

(microtextured tool, in-situ visualization and restricted contact tool), Production Engineering 16 (2022) 635–646. https://doi.org/10.1007/s11740-022-01127-w

[5] H. Klippel, S. Pflaum, M. Kuffa, K. Wegener, Automated evaluation of continuous and segmented chip geometries based on image processing methods and a convolutional neural network, Journal of Machine Engineering, 22(4) (2022) 115-132. https://doi.org/10.36897/jme/156091

[6] M. R. Chalak Qazani, V. Pourmostraghimi, M. Moayyedian, S. Pedrammehr, Estimation of tool–chip contact length using optimized machine learning in orthogonal cutting, Engineering Applications of Artificial Intelligence 114 (2022) 105118. https://doi.org/10.1016/j.engappai.2022.105118

[7] S. Arefin, X.Q. Zhang, A. Senthil Kumar, D. Wee Keong Neo, Y. Wang, Study of chip formation mechanism in one-dimensional vibration-assisted machining, Journal of Materials Processing Tech. 291 (2021) 117022. https://doi.org/10.1016/j.jmatprotec.2020.117022

[8] W. Grzesik, An integrated approach to evaluating the tribo-contact for coated cutting inserts, Wear 240 (2000) 9-18. https://doi.org/10.1016/S0043-1648(00)00324-0

[9] F. Barelli, V. Wagner, R. Laheurte, G. Dessein, Ph. Darnis, O. Cahuc, M. Mousseigne, Orthogonal cutting of TA6V alloys with chamfered tools: Analysis of tool–chip contact lengths. Proceedings of the Institution of Mechanical Engineers, Part B: Journal of Engineering Manufacture, 231 (2017) 2384-2395. https://doi.org/10.1177/0954405416629589

[10] Information on https://docs.opencv.org/4.x/d4/d13/tutorial_py_filtering.html

[11] Information on https://pyimagesearch.com/2021/04/28/opencv-smoothing-and-blurring/

[12] Information on https://docs.opencv.org/3.4/d2/d2c/tutorial_sobel_derivatives.html

[13] J. D. Bakos, Chapter 4 - Memory optimization and video processing, in Embedded Systems, 2016, pp. 147-185. https://doi.org/10.1016/B978-0-12-800342-8.00004-3.

[14] Information on https://docs.opencv.org/3.4/d7/d4d/tutorial_py_thresholding.html

[15] Information on https://docs.opencv.org/3.4/db/df6/tutorial_erosion_dilatation.html

[16] Information on https://docs.opencv.org/3.4/d4/d73/tutorial_py_contours_begin.html

[17] C. F. Jekel, G. Venter, pwlf : A Python Library for Fitting 1D Continuous Piecewise Linear Functions, MIT, 2019.